A Survey of Recombination Line Emission from the Galactic Plane at 325 MHz

K. R. Anantharamaiah *Raman Research Institute, Bangalore 560080*

Abstract. A survey of the H 272α recombination line at 325 MHz has been made towards 53 directions in the galactic plane using the Ooty Radio Telescope (ORT). 34 of these directions correspond to well-known HII regions, 12 to SNRs and 6 to 'blank' areas selected so that the 5 GHz continuum is a minimum over the telescope beam of $2° \times 6$ arcmin. Observing procedure and spectra of 47 sources towards which lines are detected are presented. Hydrogen recombination lines have been detected towards all the observed directions having $l < 40°$. Carbon recombination lines are identified in 12 of the directions. The hydrogen line intensities are found to correlate well with the total continuum intensity (which includes the nonthermal galactic background) indicating that most of the lines arise due to stimulated emission by the background radiation. A preliminary discussion on the nature of the line-emitting regions is also presented.

Key words: Galaxy, radio recombination lines—radio observations, low-frequency—stimulated emission

1. Introduction

In a heterogeneous medium, recombination line observations at different frequencies sample conditions in different components of the ionized gas (Brocklehurst & Seaton 1972; Brown, Lockman & Knapp 1978). In particular, recombination line emission at low frequencies (< 1 GHz) is expected to be dominated by low-density ionized gas and those at high frequencies by high-density gas typical of HII regions prominent in most radio continuum surveys *(e.g.* Altenhoff *et al.* 1978). This is because at low frequencies line emission from high density gas is expected to be suppressed by opacity and pressure broadening. On the other hand, recombination line emission from low-density ionized gas is expected to be enhanced at low frequencies due to stimulated emission. Calculations by Shaver (1975) have shown that at frequencies below 500 MHz stimulated emission from low-density regions can be important due to the presence of strong background continuum sources or even the nonthermal galactic background. At these frequencies, particularly strong lines can be expected from cold, partially ionized gas. Fortuitously, it is at these frequencies that both nonthermal sources and the galactic background are most intense. It appears therefore that frequencies below 500 MHz are best suited to study the conditions in cold partially ionized gas (provided the ionization is adequate) and in large low-density ionized regions for which beam dilutions are not important.

Most existing largescale recombination line surveys of the Galaxy have been carried out at frequencies higher than 1 GHz (see Wilson 1980 and references therein). Below 500 MHz there are only a handful of observations made towards a few selected sources in the galactic plane (see Pedlar & Davies 1980 and references therein). Weak centimetric wavelength recombination lines have been detected at several positions along the galactic ridge (at $l \leqslant 40°$) apparently free of discrete continuum sources (Gottesman & Gordon 1970; Gordon & Cato 1972; Matthews, Pedlar & Davies 1973; Jackson & Kerr 1975; Lockman 1976; Hart & Pedlar 1976). There are no comparable observations of these lines at frequencies below 500 MHz. The only attempt at a large-scale survey for such lines along the galactic ridge was done at 408 MHz (Batty 1976), but with very low sensitivity and which consequently did not detect any lines.

In this paper we present a survey of the H 272α recombination line (324.99 MHz) made towards 53 directions in the galactic plane using the Ooty Radio Telescope. In the next section we discuss the observing frequency and the source positions. In Section 3 we describe the equipment and observing procedure. The results of the survey and a comparison with existing low-frequency observations are presented in Sections 4 and 5. A preliminary discussion on the origin of these lines is presented in the final section.

2. Observing frequency and source positions

The rest frequency of the H 272α recombination line falls at 324.9915 MHz. A knowledge of this frequency alone allows us to put constraints on the density and emission measure of the ionized gas sampled by these observations. At this frequency the continuum optical depth of the ionized gas exceeds unity and the lines merge with the continuum when the emission measure exceeds $1.15 \times T_e^{1.35}$ pc cm^{-6}, where T_e is the electron temperature. For an electron temperature of 8000 K and a path length of about 100 pc this condition is satisfied for densities $N_e > 50$ cm^{-3}. Further, at this frequency, pressure broadening which is independent of pathlength and virtually independent of temperature (Griem 1967; Brocklehurst & Leeman 1971) considerably weakens the line intensities for $N_e > 50$ c m $^{-3}$. The brightness temperature of the nonthermal galactic background is about 600 K at this frequency and can be expected to enhance the recombination line intensities by stimulated emission in ionized gas if the density is less than a few tens cm^{-3} (Shaver 1975).

The source positions for these observations were selected from the galactic plane continuum surveys of Shaver & Goss (1970a) and Altenhoff *et al.* (1978). Most of the positions selected are in the first quadrant of the Galaxy. The galactic longitude l is restricted to $< 60°$ due to the limited declination coverage of the Ooty Radio Telescope ($-30° < \delta < 30°$).

Due to the long integration times necessary for detecting recombination lines at this frequency, a complete coverage of all the sources in the plane would require an impractical amount of telescope time. Directions were therefore selected at somewhat coarser angular intervals, but chosen so as to provide a variety of physical conditions in which to study the recombination lines. The directions selected for observations can be classified into three types.

1. *H II regions:* 34 directions corresponding to well-known HII regions of different densities and temperatures as determined by high frequency studies (*e. g.* Shaver & Goss

1970b). For reasons discussed above, the higher density HII regions are unlikely to produce detectable recombination lines at these frequencies. However, these observations can sample conditions in either low-density outer envelopes of these HII regions or low-density ionized gas which happens to be present along the line of sight.

2. *Supernova remnants:* 12 directions corresponding to well-known strong SNRs in the galactic plane. These directions are particularly suited for studying the effect of stimulated emission at low frequencies due to the strong background continuum source. There is ample evidence for the existence of substantial amounts of ionized gas along the line of sight to these sources. For example, a turnover in their continuum spectra at low frequencies has been observed (Dulk & Slee 1975). In addition, high-frequency recombination lines have been detected towards a few of these sources *(e.g.* Downes & Wilson 1974).

3. *Blank regions:* The high-resolution continuum map at 5 GHz by Altenhoff *et al.* (1978) was used to select six regions in the galactic plane devoid of any strong discrete source within the beam used for these observations. Observations in these directions are expected to provide complementary information to the galactic ridge recombination lines detected at centimetric wavelengths as mentioned above.

For comparison purposes a few positions were also selected in the anticentre direction where the nonthermal background is considerably weaker. Table 1 gives all the observed source positions in galactic and equatorial coordinates. Well-known names of the sources, where available, are indicated in column 4. The nature of the source in the direction of observation is given in column 5.

The high density of sources in the galactic plane introduces confusion. In some of the directions chosen above, the $2° \times 6$ arcmin beam intercepts more than one source. Arguments such as comparison of velocities with measurements at higher frequencies with better angular resolution should be used to identify the source of an observed line.

3. Equipment, observing procedure and data reduction

Observations were made using the 530 m $\times$ 30 m Ooty Radio Telescope (ORT) (see Swarup *et al.* 1971 for a detailed description). Since these are the first major spectral line observations carried out with the ORT, we describe in some detail below the equipment, observing procedure and the difficulties encountered in using such a phased-array telescope for line studies. We begin with a brief description of the ORT.

The ORT operates at a nominal centre frequency of 326.5 MHz and has an angular resolution of $2°$ in RA and 5.6 sec δ arcmin in declination. The telescope is equatorially mounted and mechanically steerable to track a source continuously for about 9 hours, a feature particularly suited for these observations since long integration times are required. The beam is steered in declination using phase shifters at RF of 326.5 MHz and delays and phase shifters at an IF of 30 MHz (Sarma *et al.* 1975). With the new RF amplifiers and phase shifters installed recently, the system temperature at the input of the RF amplifier is now about 300 K when the antenna is pointed towards a cold region in the sky. A source of 1 Jy in the beam of the antenna produces an increase of about 1.8 K in this system temperature.

The back-end is a 128 channel one-bit autocorrelator which can analyse total bandwidths of 500 kHz, 250 kHz and 125 kHz. After Hanning smoothing of the

Table 1. Source positions and continuum temperatures.

Galactic coordinates l b	RA(1950) h m s	DEC(1950) ° ' "	Source name	Source type	Telescope[2] configuration	Total Continuum Temperature[1] K
(1)	(2)	(3)	(4)	(5)	(6)	(7)
357.7 −0.1	17 36 57	−30 56 41	...	SNR	A	930
359.9 −0.0	17 42 27	−28 59 04	SGR A	Gal. centre	A	2330
0.7 −0.0	17 44 10	−28 21 59	SGR B2	H II	A	1100
2.1 −0.0	17 47 27	−27 07 29	...	Blank	B	740
2.3 +0.2	17 46 56	−26 49 35	...	H II	B	750
4.2 −0.0	17 52 14	−25 18 49	...	Blank	B	690
4.4 +0.1	17 52 13	−25 04 52	AMW 35	H II	A	700
6.0 −1.2	18 00 33	−24 23 25	M 8	H II	D	660
6.6 −0.1	17 57 54	−23 21 17	W 28	SNR	D	900
7.0 −0.3	17 59 17	−23 02 54	M 20	H II	A	720
8.1 +0.2	17 59 55	−21 48 17	...	H II	A	770
9.4 +0.1	18 03 03	−20 45 22	...	Blank	C	730
10.2 −0.3	18 06 25	−20 19 42	W 31	H II	D	610
10.3 −0.2	18 05 60	−20 05 52	...	H II	B	680
11.2 −0.3	18 08 31	−19 26 31	...	SNR	A	760
12.8 −0.2	18 11 10	−17 57 56	W 33	H II	A	730
14.0 −0.1	18 13 26	−16 51 55	...	H II	A	680
15.1 −0.7	18 17 35	−16 12 22	M 17	H II	D	810
15.7 −0.0	18 16 24	−15 17 58	...	Blank	C	610
16.9 +0.7	18 16 08	−13 51 41	M 16	H II	C	610
17.6 −0.3	18 21 17	−13 44 04	...	Blank	C	630
18.9 −0.5	18 24 21	−12 44 28	...	H II	A	660
19.6 +0.0	18 23 56	−11 52 40	...	H II	D	550
20.7 −0.1	18 26 26	−10 54 53	...	H II	A	590
21.2 −0.0	18 27 01	−10 28 09	...	Blank	B	580
21.8 −0.6	18 30 25	−10 12 46	...	SNR	A	790
23.0 −0.3	18 31 27	−08 57 27	W 41	SNR	A	770

l	b	RA (h m s)	Dec (° ′ ″)	Source	Type	Module	T_B
23.4	−0.2	18 31 57	−08 35 51	...	H II	A	750
24.8	+0.1	18 33 29	−07 13 10	...	H II	A	660
25.4	−0.2	18 35 31	−06 50 32	3C 385	H II	A	650
27.3	+0.2	18 37 53	−05 00 47	...	H II	A	640
28.8	+3.5	18 28 48	−02 07 37	W 40	H II	A	450
29.9	+0.0	18 43 30	−02 44 01	...	H II	B	650
29.9	−0.2	18 43 25	−02 43 47	...	H II	A	680
30.8	+0.0	18 44 50	−01 59 04	W 43	H II	C	830
31.9	+0.0	18 46 51	−00 58 52	3C 391	SNR	A	680
34.6	−0.6	18 53 57	+01 06 20	W 44	SNR	A	830
34.7	−0.6	18 54 13	+01 14 24	W 44	SNR	A	950
35.1	−1.6	18 58 43	+01 08 24	W 48	H II	A	460
37.8	−0.2	18 58 30	+04 09 54	W 47	H II	D	480
39.2	−0.3	19 01 35	+05 21 35	3C 396	SNR	A	570
39.7	−2.2	19 09 21	+04 53 48	W 50	SNR	B	360
43.2	−0.1	19 08 16	+08 59 54	W 49	SNR	A	690
45.4	+0.1	19 11 57	+11 03 41	...	H II	B	360
49.0	−0.3	19 20 17	+14 02 01	W 51B	H II	A	650
49.0	−0.6	19 21 23	+13 51 51	W 51C	SNR	D	490
49.5	−0.4	19 21 27	+14 24 22	W 51A	H II	A	450
51.4	+0.0	19 23 42	+16 14 17	...	H II	A	290
54.1	−0.1	19 29 27	+18 35 52	...	H II	A	210
59.9	+0.2	19 40 24	+23 42 32	...	H II	A	120
206.0	−2.1	06 28 29	+05 13 25	W 16	H II	A	100
206.8	−16.4	05 39 11	−01 55 50	NGC 2024	H II	A	120
209.2	−19.4	05 32 50	−05 25 09	Orion A	H II	A	420

Notes:

1. Total beam-averaged brightness temperature. Error on the measurement of this quantity is estimated to be 15 per cent.

2. The 530 m × 30 m Ooty radio telescope is divided into 22 equal modules along the north-south direction. Starting from the middle the northern modules are designated as N1, N2 ... N11 and southern modules as S1, S2 ... S11. Signals from each of the modules are brought independently into the receiver room and combined with proper phases and delays to form the final beam. There is provision to switch off any of the modules thereby removing their contribution to the final output. These observations were made during the period when the telescope was undergoing major modifications. Therefore many sources in this list were observed with one or more modules switched off. Switching off modules starting from either end reduces the collecting area and broadens the beam. Switching off intermediate modules creates a hole in the aperture, reducing the collecting area and introducing low-level side lobes. For the purpose of this table the designations in this column mean the following: A—All modules on, B—N1 module off, C—N1 and N2 modules off, and D—Modules S6 to S11 off.

autocorrelation function, these bands can provide frequency resolutions of 7.8 kHz, 3.9 kHz and 2.0 kHz respectively. Any required frequency band at the RF can be placed in the autocorrelator band by changing the frequency of a synthesizer used as the first local oscillator (FLO).

Observations were made in the total power mode in several sessions during the period from August 1980 to May 1982. During this period the ORT was undergoing several modifications in its front-end system. Therefore some of the observations were made with some sections of the telescope missing, and sometimes with slightly different sensitivity. Column 6 of Table 1 indicates the configuration of the telescope during the different observations. However during all the observing sessions the line intensities were measured with respect to the adjacent continuum, which to first order removes the dependence on system parameters. A bandwidth of 500 kHz (which corresponds to ~ 461 km s^{-1} at the H 272α frequency) was used during all the observations providing a velocity resolution of 7.2 km s^{-1}. Double frequency switching was employed for all the observations; the FLO was switched between the line frequency (ON) and two reference frequencies (REF1, REF2), one on either side in the sequence ON-REF1-ON-REF2-ON-*etc*, spending 0.25 seconds at each frequency. Depending on the direction of observation, the line frequency was chosen such that the expected LSR velocity of hydrogen and carbon 272α lines fell within the observing band.

The different frequency settings of the FLO and switching between them which is necessary for these observations, introduces many complications in the performance of the antenna and the receiver. When the frequency of the FLO is changed from the nominal setting of 296.5 MHz by an amount Δf, the north-south pointing of the antenna changes by an amount $\Delta\delta = (\Delta f / f) \tan \delta$, where f is the nominal RF centre frequency (326.5 MHz) of the system. Therefore, when the central frequency of observation is changed from the nominal setting (for example to the H 272α frequency) a set of systematic phase corrections have to be applied in order to point the antenna in the desired direction. We find that a change in the centre frequency also decreases the sensitivity of the system; the sensitivity drops by about 20 per cent at the frequency of the H 272α line. This may be partly due to problems in applying phase corrections in the system.

A further complication is introduced when the FLO is switched between the line and reference frequency. The corresponding beamshift produces a change in the total system temperature whose magnitude depends on the strength, size and angular distribution of the source being observed. A mere change in the total system temperature, which only introduces a change in the input signal level, does not change the response of a one-bit correlator. However, this change in the system temperature is really a function of frequency even within the bandwidth of 500 kHz. This produces a curved baseline in the final spectrum obtained by subtracting the line and reference band shapes and dividing by the reference band shape. The curvature of the baseline is therefore a function of the continuum distribution of the source being observed. This being so, we cannot use observations towards a reference region to remove the instrumental baseline as is done in many single-dish spectral-line observations. We were able to minimize the baseline curvature by using double frequency switching as described above. We tried to reduce the curvature further by also switching in phase corrections, as mentioned above, corresponding to the line and reference frequencies. Phase correction switching considerably reduced the total system temperature variation but failed to improve the baseline; in fact in some cases the curvature in the

baseline deteriorated. Several test observations towards a cold region in the sky showed that the instrumental baseline introduced only by the frequency response of the RF amplifiers is minimal.

In Fig. 1 we show examples of two baselines. SgrA, the strongest source in these observations, has a sharply peaked continuum distribution and is an example of the most unfavourable baseline. A fourth-order polynomial has been fitted to channels devoid of line emission to determine the instrumental baseline. However, the baseline for most of the sources are intermediate between SgrA and W 41 shown in Fig. 1. Polynomials up to third order were fitted to determine the baselines in most of the cases. In a few cases a fourth-order polynomial was necessary.

Each source was observed in three to four sessions either on successive days or separated by several days depending on the availability of telescope time. Data were acquired in stretches of 1 to 1.5 hours while tracking the source position over an hour-angle range generally between -4^h and $+4^h$ 30^m. Individual scans were combined, after
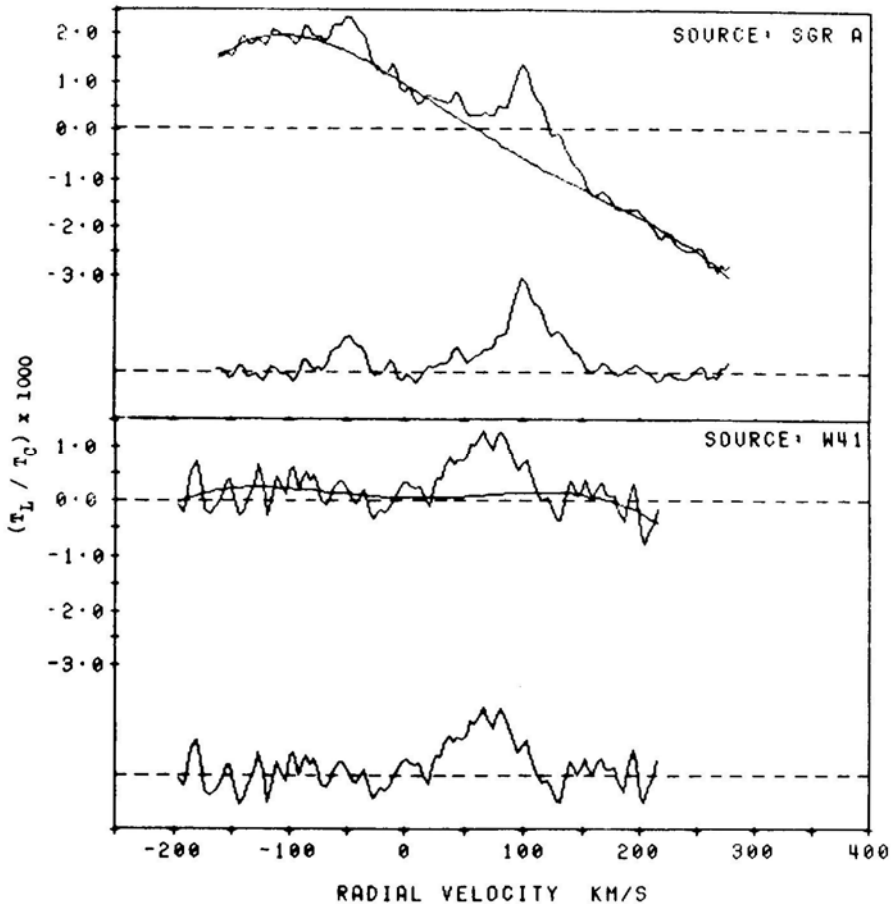

Figure 1. Observed spectra and the fitted instrumental baseline towards two sources Sgr A and W 41. The spectrum in the lower part of both the frames is obtained after subtracting the baseline shown as a solid line

editing out interference, to form a one day's spectrum for the source. A one-bit auto-correlator only measures a normalized spectrum (Weinreb 1962). At the beginning of each day's observing session the increase in the total system temperature at the source position was measured with respect to a region generally about $1^h.5$ to 2^h away in right ascension. This was used to calibrate each day's spectrum in terms of the line to continuum ratio. These one day spectra for each source were averaged with weighting functions proportional to their integration times to obtain the final spectrum for the source. Instrumental baselines were fitted and removed from these final spectra as described above. For some sources the data were further smoothed to improve the signal-to-noise ratio. It was ensured that the smoothing process did not affect any narrow feature. For most of the sources, gaussian components were fitted to the line profiles using a standard least-square technique and the line parameters were determined. In Fig. 2 we show an example of a gaussian fit and the residuals after subtracting the fitted components from the final spectrum. In all the cases, the residuals obtained this way showed rms noise fluctuations consistent with that expected for a one-bit correlator (Weinreb 1962). The source G 359.9 – 0.1 (SgrA) was observed several times during the one-and-half year period of these observations to monitor the satisfactory functioning of the system at all times. This resulted in a particularly long integration time and therefore the best signal-to-noise ratio for this source.

One of the major difficulties in spectral-line-observations at low frequencies is the presence of CW interference. Low-level CW interference from equipment in the laboratory, low-level oscillations in one of the RF amplifiers, harmonics of transmissions in the communication bands from nearby ground-based transmitters and satellites, can all seriously affect the quality of the data. In fact, for some period during
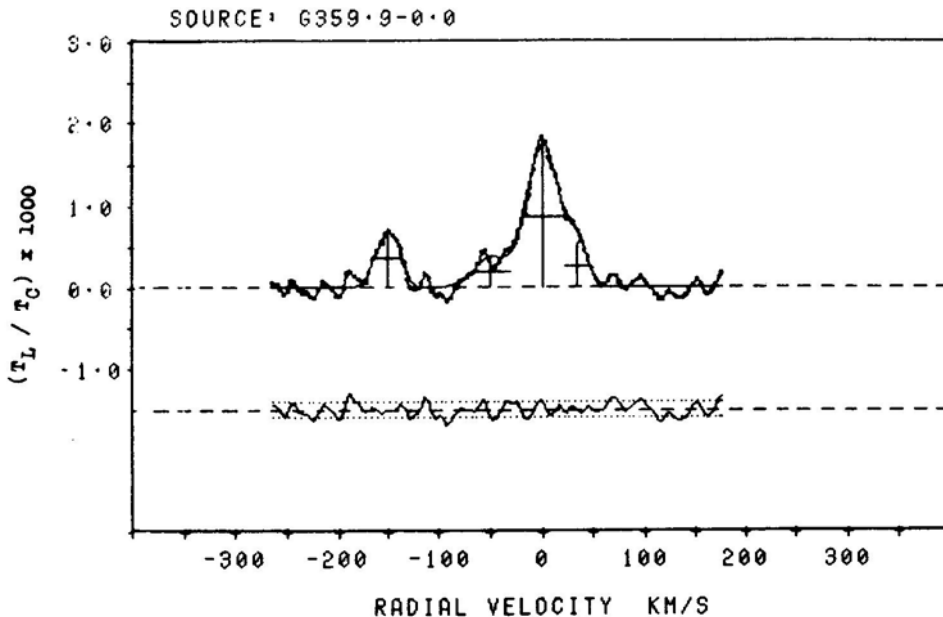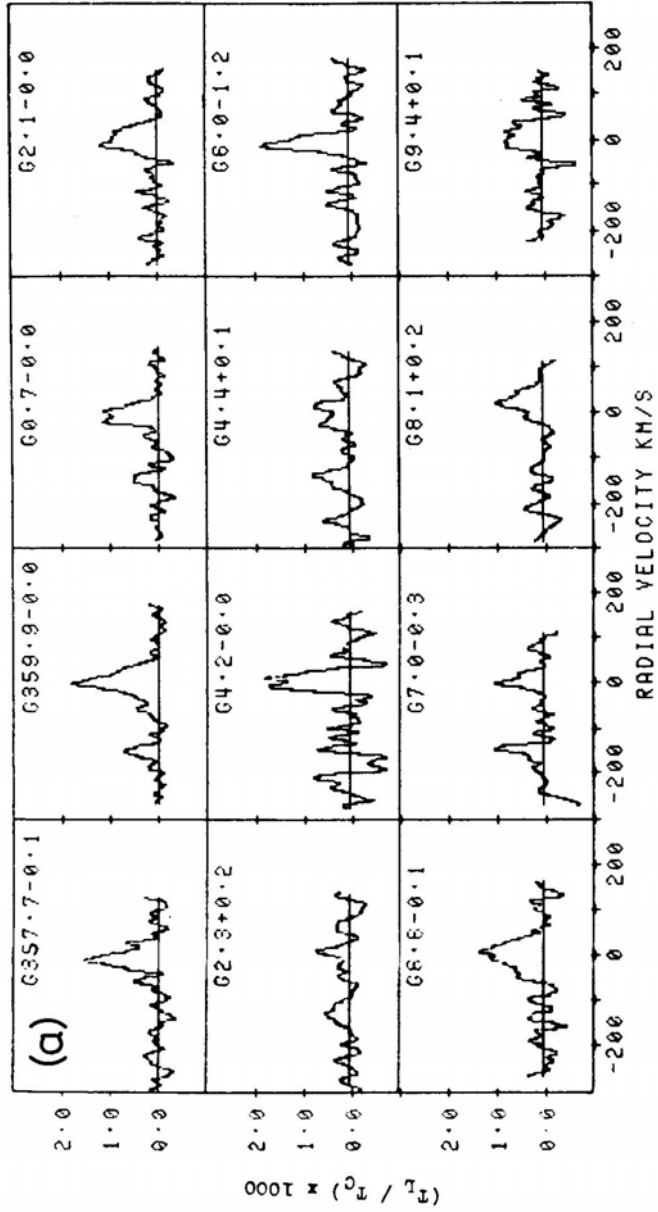

Figure 2. An example of a gaussian fit to the final spectrum. The crosses indicate the amplitude and width (FWHM) of the fitted components. The residuals after removing the gaussians are also shown. The dotted lines indicate the expected 1σ amplitude of the residuals.
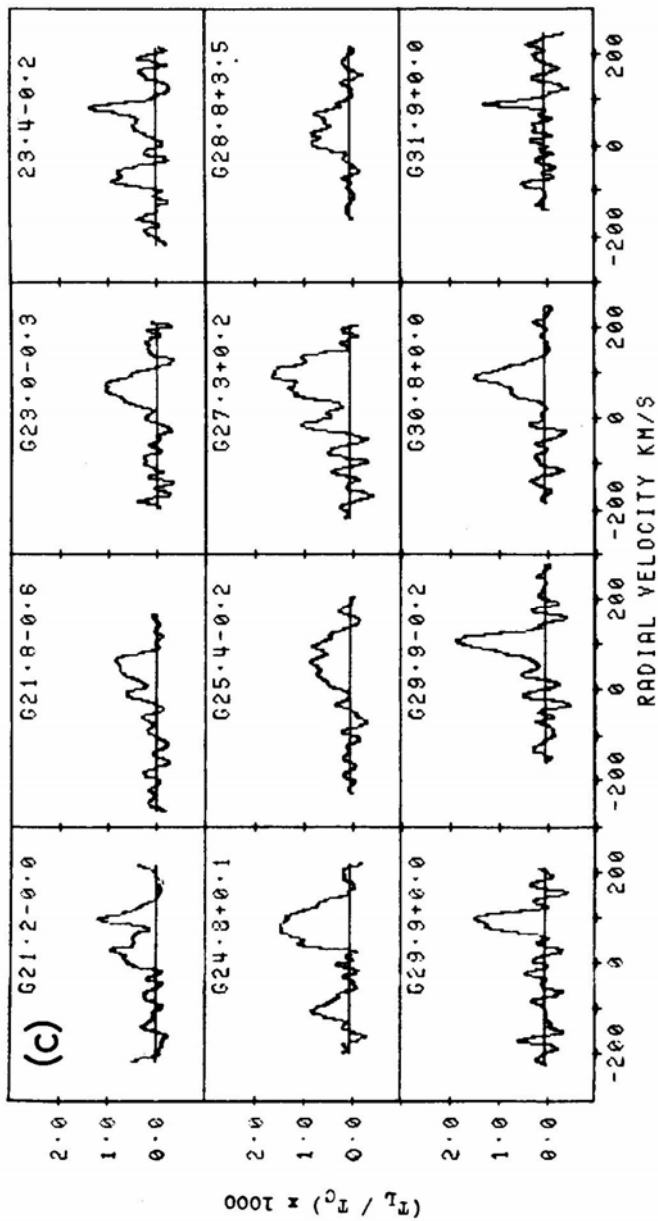
these observations, strong interference through the image band of the ORT receiver (266.5 MHz) was coming from a geostationary satellite. Because of this, after some initial observations at the H 271α recombination line frequency (328.6 MHz), we switched to the H 272α line at 324.99 MHz. The interference usually manifests itself as an increase in the rms noise in the spectra, or as sharp spikes in either one-minute data or in the averaged spectrum depending on the strength and duration. The 'lines' due to interference can generally be easily distinguished from those due to an astronomical source by their peakiness and confinement to one or two channels only. In the final analysis, all such stretch of data containing this type of interference were deleted. Up to 30 per cent of the total acquired data had to be discarded due to the presence of such interference. We have carefully examined all the individual pieces of data making up the final spectrum for each source to ensure that the line emission attributed to an astronomical source is not due to the presence of interference in some individual stretches of data. Except for the sources W 51B and Orion, we believe that all the data presented here are free of interference to a high degree.

Continuum measurements of all the sources observed for recombination lines were made in a separate session in 1983 April. Even though the observed lines were already calibrated in terms of line-to-continuum ratios, the continuum measurements were necessary for interpretation since the total background radiation can cause stimulated emission of these lines as discussed before. For each of the source positions the increase in total system temperature was measured with respect to a cold region about $2^h.5$ to 3^h away in right ascension. This was compared with the increase in system temperature due to the sources 3C 283 and Her-A. The flux density of 3C 283 at 327 MHz was taken to be 20.6 Jy and that of Her-A as 200 Jy. Necessary corrections were applied for the deviation of the total power detector characteristic from a true square law. The resulting equivalent flux in the beam was converted to average beam brightness temperature using the measured main-beam solid angle of the ORT. No attempt was made to separate the contributions from the source in the beam and the background. The measured beam brightness temperature for each source is given in Column 7 of Table 1.

4. Results

Out of the 53 directions observed, recombination lines have been detected in 47 directions. The observed spectra corresponding to directions in which lines were detected are presented in Fig. 3 in which the ratio of line to total underlying continuum intensities have been plotted against radial velocity with respect to LSR calculated using the rest frequency of the H 272α recombination line. The line parameters obtained from a least-squares gaussian fit to the observed profiles are given in Columns 2 to 4 of Table 2. Columns 5 and 6 of this table give the velocity resolution of the spectra and the integration time respectively. The peak brightness temperature of the line T_{BL} is given in Column 7. This was obtained by multiplying the quantity in Column 2 by the measured continuum beam brightness temperature for the source indicated in Column 7 of Table 1. For many of the sources (particularly those with very wide lines), the individual line parameters obtained from gaussian fits can only be used as indicators of the strength and extent of the line; a single gaussian component may not accurately represent the true line shape. A more meaningful parameter would be the integrated

Figure 3. H 272α spectra of sources towards which lines were detected. The radial velocity is with respect to LSR. T_L is the antenna temperature in the line and T_C is that in the continuum which includes the nonthermal galactic background.
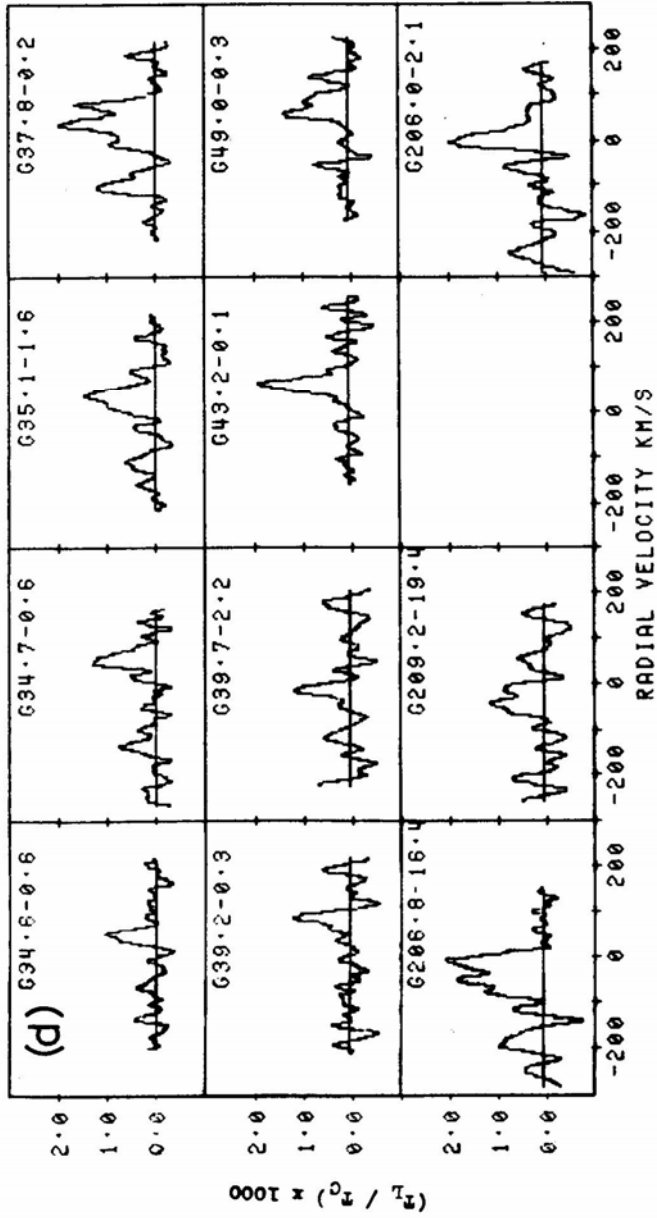
Figure 3. Continued. The ordinate scale for the source G 206.0 − 2.1 is $(T_L/T_C) \times 500$.

Table 2. Observed line parameters and integration times.

Source	H 272α gaussian parameters			Spectral Resolution km s⁻¹	Integration time hours	Peak line temperature T_{BL} (K)	$\int T_{LB}\,dv$ K kHz	Velocity of H 110α[1] km s⁻¹	$V_{110\alpha} - V_{272\alpha}$[1] km s⁻¹
	Peak $T_L/T_C \times 10^3$	Width (FWHM) km s⁻¹	Velocity (LSR) km s⁻¹						
1	2	3	4	5	6	7	8	9	10
G 357.7 − 0.1	1.39(09)	40(3)	−7.9(1.3)	10	25.9	1.3(2)	60(11)	⋮	⋮
G 359.9 − 0.0	1.59(04)	51(1.5)	4.7(0.6)	10	62.5	3.7(6)	238(35)	18	13
	0.36(06)	21(4.5)	−57(2)			0.8(2)			
	0.71(06)	24(2.5)	−149.5(1.0)*			1.7(3)			
G 0.7 − 0.0	1.13(06)	43(3)	−4.4(1.2)	12	22.9	1.24(20)	46(9)	64.6	69
	0.58(09)	20(4)	−146(2)*			0.64(14)	62(11)		
G 2.1 − 0.0	1.10(07)	47(4)	5(2)	12	33.8	0.81(13)	15(4)	⋮	⋮
G 2.3 + 0.2	0.64(13)	18(5)	9(2)	15	19.3	0.48(12)	44(8)	5.0	−4
	0.48(10)	36(9)	−127(4)			0.36(09)	10(4)		
G 4.2 − 0.0	1.9(2)	33(5)	7(2)	12	12.0	1.28(24)	15(5)	⋮	⋮
G 4.4 + 0.1	0.56(09)	66(13)	4(5)	15	19.0	0.39(09)	49(11)	5.7	2
	0.70(13)	26(7)	−141(3)*			0.49(12)	30(9)		
G 6.0 − 1.2	1.83(14)	26(3)	−4(1)	15	11.9	1.2(2)	15(5)	3.0	7
G 6.6 − 0.1	1.2(1)	43(4)	11(2)	12	14.4	1.1(2)	36(7)	12.5	2
	0.36(10)	41(13)	−27(6)			0.32(10)	69(12)		
G 7.0 − 0.3	0.87(13)	30(6)	6(2)	15	10.0	0.63(13)	22(6)	14.0	8
	1.0(2)	14(4)	−144(2)*			0.73(16)	12(4)		
G 8.1 + 0.2	0.83(09)	47(7)	25(3)	20	16.0	0.64(12)	35(8)	22	−3
G 9.4 + 0.1	0.83(12)	42(7)	10(3)	12	24.6	0.61(13)	30(8)	⋮	⋮
G 10.2 − 0.3	1.27(08)	51(4)	15(2)	15	13.6	0.77(13)	45(8)	13.0	−2
G 10.3 − 0.2	1.36(12)	29(3)	32(2)	15	12.0	0.92(16)	31(6)	12.0	−20
G 11.2 − 0.3	1.1(2)	23(6)	37(2)	15	8.3	0.8(2)	22(7)	⋮	⋮
G 12.8 − 0.2	1.0(1)	32(4)	26(2)	15	12.0	0.72(13)	27(6)	30.0	4
G 14.0 − 0.1	1.4(1)	38(3)	24.1(1.5)	15	11.7	1.0(2)	43(8)	31.5	7
	1.1(1)	29(4)	−122(2)*			0.74(14)	25(6)		
G 15.1 − 0.7	0.83(07)	41(5)	9(2)	20	18.7	0.67(12)	32(7)	11.5(3)	

Source									
G 15.7−0.0	1.4(1)	58(5)	43(2)	12	19	0.86(14)	58(11)	...	...
G 16.9+0.7	1.19(06)	53(3)	20(1)	12	27.8	0.73(11)	45(7)	28.0	8
G 17.6−0.3	1.07(08)	47(4)	30(2)	15	20.4	0.67(11)	36(7)	...	...
	0.32(08)	50(15)	−129(6)*			0.20(06)	12(5)	...	...
G 18.9−0.5	1.6(2)	32(4)	48(2)	15	13.2	1.0(2)	38(9)	67	19
G 19.6+0.0	1.3(1)	35(3)	41(2)	15	16.7	0.71(12)	29(6)	55.3	14
	0.67(14)	13(5)	−100(2)*			0.37(09)	6(2)	...	...
G 20.7−0.1	0.77(14)	19(6)	47(3)	20	9.9	0.45(11)	10(4)	57	10
G 21.2−0.0	1.11(10)	26(3)	98.6(1.3)	15	20.5	0.64(11)	48(7)	...	...
	0.80(07)	54(6)	25(3)			0.46(08)		...	...
G 21.8−0.6	0.89(08)	44(5)	54(2)	20	13.7	0.70(12)	43(8)	...	...
	0.62(12)	13(5)	−9(2)			0.49(12)		...	...
G 23.0−0.3	1.09(07)	55(4)	68(2)	12	18.7	0.84(14)	53(10)	78.0	10
G 23.4−0.2	1.30(14)	27(4)	85(2)	15	14.5	1.0(2)	31(7)	104.0	19
	0.93(13)	30(6)	−64(2)*			0.70(14)	24(7)	...	...
G 24.8+0.1	1.51(06)	77(4)	83(2)	15	15.4	1.00(15)	89(14)	107.0	24
	0.73(09)	34(5)	−104(2)*			0.48(09)	19(5)	...	...
G 25.4−0.2	0.78(06)	95(9)	64(4)	20	14.7	0.51(09)	56(11)	59.0	−5
G 27.3+0.2	1.53(09)	85(6)	93(2)	15	14.1	0.98(16)	110(18)	33.0	−60
	1.0(2)	18(5)	−12(2)			0.65(15)		...	45
G 28.8+3.5	0.61(06)	35(4)	72(2)	15	17.5	0.27(05)	29(4)	0.7[2]	−72
	0.79(05)	44(4)	19(2)			0.36(06)		...	−19
G 29.9+0.0	1.51(13)	35(4)	91(2)	15	13.0	1.0(2)	40(8)	98.5	8
G 29.9−0.2	1.86(12)	37(3)	105(2)	15	21.8	1.26(21)	54(10)	...	...
G 30.8+0.0	1.42(08)	41(3)	95(1)	15	20.5	1.2(2)	64(11)	90.0	−5
	0.55(12)	16(5)	54(2)			0.46(12)		...	...
G 31.9+0.0	1.3(2)	10(2)	98(1)	12	22.2	0.9(2)	10(3)	103[4]	5
G 34.6−0.6	1.05(11)	21(3)	48(1)	12	13.0	0.87(16)	21(5)	53.0	5
G 34.7−0.6	1.24(10)	37(4)	59(2)	12	14.3	1.2(2)	50(10)	50.3[3]	−9
	0.69(13)	20(5)	−132(2)*			0.7(2)	15(5)	...	...
G 35.1−1.6	1.33(12)	55(6)	34(3)	15	13.4	0.61(11)	39(8)	43.0	9
G 37.8−0.2	1.59(11)	81(6)	48(3)	15	16.9	0.76(13)	71(13)	61.0	13
	1.2(2)	26(5)	−96(2)*			0.57(12)	17(5)	...	...
G 39.2−0.3	1.15(14)	21(5)	84(2)	15	11.3	0.66(13)	16(5)	...	...
G 39.7−2.2	1.1(2)	18(6)	−11(3)	20	17.5	0.4(1)	9(4)	...	...
G 43.2−0.1	1.72(11)	35(3)	63(1)	12	28.1	1.2(2)	48(9)	10.0	−53

Table 2. Continued.

Source	Peak $T_L/T_C \times 10^3$	Width (FWHM) km s^{-1}	Velocity (LSR) km s^{-1}	Spectral Resolution km s^{-1}	Integration time hours	Peak line temperature T_{BL} (K)	$\int T_{LB}\,dv$ K kHz	Velocity of H110α[1] km s^{-1}	$V_{110\alpha} - V_{272\alpha}$ km s^{-1}
1	2	3	4	5	6	7	8	9	10
G 45.4+0.1	<1.6	...	...	15	15.5	<0.6	...	54.5	...
G 49.0−0.3†	1.1(1)	55(6)	75(3)	15	15.8	0.75(15)	46(10)	60.5	−14
G 49.0−0.6	<1.3	...	...	15	11.3	<0.7	...	...	...
G 49.5−0.4	<1.0	...	...	15	22.5	<0.5	...	57.1	...
G 51.4+0.0	<2.1	...	...	20	11.0	<0.6	...	53.3	...
G 54.1+0.2	<1.6	...	...	20	10.0	<0.3	...	43.0	...
G 59.8+0.2	<4.0	...	...	20	12.2	<0.8	...	−6	...
G 206.0−2.1	4.0(5)	28(5)	5(2)	20	32.3	0.4(1)	13(3)	7(3)[5]	2
G 206.8−16.4†	1.78(12)	84(7)	−36(3)	15	112.9	0.21(04)	20(4)	7.0[2]	43
	1.0(2)	26(7)	−187(3)*			0.12(03)	4(1)		
G209.2−19.4†	1.0(2)	53(11)	−34(5)	20	23.2	0.43(10)	26(8)	−2.7[2]	31

Notes:

1. From Downes *et al.* (1980)
2. Velocity of 109α line form Reifenstein *et al.* (1970)
3. Velocity of 166α line form Bignell (1973)
4. Velocity of 92α line form Cesarsky & Cesarsky (1973)
5. Velocity of 100α line from Viner, Vallée & Hughes (1979)
* Possible carbon line
† Observations affected by interference

line intensity. This quantity computed from the gaussian parameters for each source is given in Column 8 of Table 2. Possible carbon lines have been excluded when obtaining this quantity. The errors quoted in Table 2 are equal to one standard deviation. These errors are obtained from the rms noise of the residuals after gaussian fit and using the formulae relating this noise to the error of the parameters as discussed by Rieu (1969).

The main results of this survey can be summarized as follows.

1. In the first quadrant of the Galaxy, for the longitude range $l \leqslant 40°$, hydrogen recombination lines were detected towards every direction irrespective of whether it corresponded to an HII region or an SNR or a blank region. Outside this range the line was detected only towards two strong sources W 49 and W 51. The line was also detected towards the three HII regions in the anticentre direction.

2. The line intensities are typically about 0.1 per cent of the total continuum intensity, and required integration times ranging from 10 hours to 30 hours for detection with a signal-to-noise ratio between 5 and 10.

3. There is no marked difference in the line to total continuum intensity ratio between directions of HII regions, SNRs and blank regions.

4. Typical widths of the lines (FWHM) are 20–50 km s^{-1}. However, the spectrum is much wider (60–80 km s^{-1}) or has more than one component for many sources, particularly those in the longitude range 20° to 30°. The line towards 3C 391 (G 31.9 + 0.0) is particularly narrow; the FWHM is only about 11 km s^{-1} after correction for instrumental broadening.

5. The strongest H 272α line detected is towards the galactic centre. The line profile clearly shows three components; one centred at 0 km s^{-1} one around – 50 km s^{-1} and the other at a positive velocity.

6. Judging by the frequency shift ($\sim$ 162 kHz $\simeq$ 149 km s^{-1}) with respect to the hydrogen line, carbon lines can be identified in about 12 cases. These lines are however somewhat wider (20–30 km s^{-1}) than the carbon lines observed at higher frequencies (5–15 km s^{-1}).

5. Comparison with other low-frequency observations

Recombination lines from a few individual sources in this survey have been observed before by other workers using other telescopes at frequencies below 500 MHz. For comparison we have selected all those sources in Table 1 which have been observed at frequencies close to that of this survey. The frequency of observation, angular resolution, observed line parameters and references are given in Table 3. Comparison of these parameters with those given in Table 2 for the same sources show that the observed line intensities and centroids are in good agreement for most of the sources; the slight differences in these quantities could be the result of the very different beam sizes employed for the two observations. Some noticeable differences between the two sets of observations are described below.

The width of the line towards the SNR 3C 391 (G31.9 + 0.0) observed at this frequency is much smaller than at higher frequencies. On the other hand, the lines towards SgrA and M 17 are somewhat broader. The observations towards W 5IB at 325 MHz seem to show additional components at higher velocities. But these components have to be treated with, caution since, as noted earlier, observations towards this source were affected by interference. Further, we have not detected any

Table 3. Parameters from other observations for comparison.

Source	Name	Frequency MHz	Size arcmin	T_L/T_C ×10³	T_C K	T_L K	Width km s⁻¹	V_{LSR} km s⁻¹	Reference
G 359.9 − 0.0	SGR A	328	50	1.5	1770	2.6(0.4)	26(5)	2.1(1.5)	1
G 15.1 − 0.7	M17	386	35	1.0	527	0.5(0.2)	24(17)	15	2
				1.1		0.6(0.1)	34(20)	51	
G 30.8 − 0.0	W 43	328	50	2.4	380	0.9(0.4)	48(11)	102(10)	1
G 31.9 + 0.0	3C 391	428	11	2.5	466	1.15	63	90	3
G 43.2 + 0.0	W 49A	318	16	3.0	250	0.75(0.2)	25(8)	62(6)	4
G 49.0 − 0.3	W 51B	318	16	2.3	860	2.0(0.3)	25(9)	60(7)	4
G 49.0 − 0.6	W 51C	430	9	3.2(0.8)			15(4)	56(2)	5
G 49.5 − 0.4	W 51A	428	11	1.8(0.3)	530		31(7)	55(3)	6
G 206.1 − 2.3	W 16	386	36	3.8	89	0.34(0.12)	38(15)	16	2

1. Pedlar et al. (1978)
2. Gordon, Gordon & Lockman (1974)
3. Pankonin (1975)
4. Parrish, Conklin & Pankonin (1977)
5. Terzian & Pankonin (1974)
6. Pankonin et al. (1974)

lines towards W 51C and W 51A and our upper limits are somewhat lower than the intensities reported by Terzian & Pankonin (1974). Again, some of these differences may be due to the different angular resolution, frequency and sensitivity of the two sets of observations.

6. Discussion

Detailed interpretation of the data presented in this paper in terms of the distribution and properties of the gas responsible for the observed lines will appear in subsequent publications. Here we discuss only the broad characteristics of the data and their implication for the nature of the line-emitting regions.

6.1 *Hydrogen Lines*

6.1.1 *Line Intensities*

As discussed earlier, there combination lines observed at this frequency can only sample conditions in relatively low-density ionized regions. Macroscopic properties of a large selection of HII regions in the galactic plane have been studied by Shaver & Goss (1970b). Most of the HII regions common to the present H 272α recombination line survey and the continuum survey of Shaver & Goss (1970b) have electron densities greater than 100 cm^{-3} and angular sizes less than 10 arcmin. With these densities and sizes, effects of pressure broadening, optical depth and beam dilution make the recombination lines at this frequency virtually undetectable from these HII regions. The recombination lines measured here must therefore arise from much lower-density gas in regions of much larger angular size. The gas can either be associated with the HII region, for example as an outer envelope, or just lying along the line of sight. Further, the intensity and width of the recombination lines detected in this survey are very similar in all directions observed, irrespective of whether the direction corresponds to that of an HII region, an SNR or a blank region. The intensities of the lines are found to correlate well with the total continuum intensity. In the galactic plane where most of these observed sources lie, the continuum radiation at this frequency is mainly nonthermal in origin. Therefore, the line and continuum radiation originate in different regions along the line of sight. The HII regions and SNRs only add to the background continuum radiation, and the lines themselves must arise in low-density ionized regions distributed along the line of sight. The ORT beam of $2° \times 6$ arcmin and the low observing frequency are probably well suited for studying the properties of such low-density ionized gas not prominent in the continuum. At higher frequencies, where better angular resolutions are available and where the expected intensity of recombination lines from the HII regions themselves are much higher, it would be difficult to separate the contribution from lower-density gas.

6.1.2 *Stimulated Emission*

Stimulated emission of recombination lines due to non-LTE populations of high principal quantum number levels is expected to be important at low frequencies (Shaver 1975). The presence of a strong background source or even the nonthermal
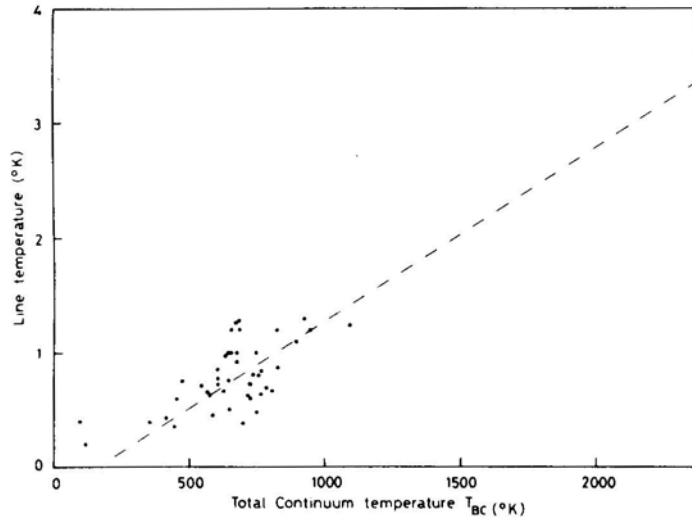
Figure 4. Correlation of the line temperature with the total continuum temperature which includes the nonthermal galactic background. The dashed line indicates the least squares fit. Correlation coefficient is 0.8.

galactic background is expected to have considerable influence on the line intensities Pedlar *et al.* (1978) have demonstrated that the intensity of the low-frequency recombination line towards the galactic centre is enhanced by the background continuum sources in that direction. In Fig. 4 we have plotted the peak line brightness temperature T_{BL}, observed in different directions, against the total continuum temperature T_{BC} which includes the nonthermal galactic background. There is a good correlation between them (correlation coefficient = 0.8) indicating that the line intensities are enhanced by the background radiation. It may be noted here that such a correlation between line and continuum intensity has been observed even at 5 GHz (Jackson & Kerr 1975). But at this frequency the continuum is mainly thermal, and the correlation is expected even in the absence of stimulated emission. However, at low frequencies (< 500 MHz) the continuum intensity is dominated by the nonthermal emission and any correlation between T_{BL} and T_{Bc} can only be due to stimulated emission.

6.1.3 *The Line Velocities*

The radial velocity with respect to LSR for all the observed lines is given in Column 4 of Table 2. The measured radial velocity of an object in the galactic plane is an indicator of its location along the line of sight. It is useful to compare the velocity of the H 272α line observed here with that of a higher-frequency recombination line, as the latter arises preferentially in the relatively high-density HII regions along the line of sight. Column 9 of Table 2 gives the velocity of the H 110α observed by Downes *et al.* (1980) in the same directions. Column 10 is the difference between the observed H 272α velocity and the H 110α velocity. A histogram of these differences is shown in Fig. 5. These differences are an indication of the separation along the line of sight between the HII
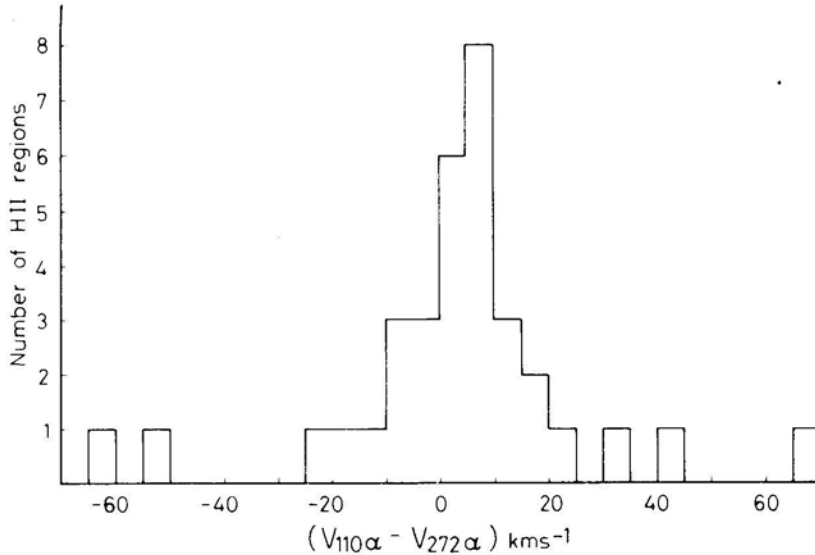
Figure 5. Histogram of the difference between the observed velocity of the H 272α line and the H 110α line in the same direction (see Column 10 of Table 2).

regions from which the H 110α line is observed and the lower-density gas from which the H 272α line is observed. The histogram in Fig. 5 shows that in the 60 per cent of the cases the difference in velocity is within 10 km s^{-1}. Within the observational errors (which are 2–5 km s^{-1} for both) the velocities are in good agreement. In any case there is always a substantial emission of the H 272α line at the velocity of the HII region (as seen in H 110α line) in more than 90 per cent of the cases. This clearly suggests that the low-density gas responsible for the H 272α line is associated with the dense HII region in that direction. In those cases where the velocity difference is large the two regions must be physically widely separated, unless there is differential motion between the higher- and lower-density regions.

6.1.4 *The l–v Diagram*

The longitude velocity (*l–v*) diagram of the lines observed is an indicator of the distribution of the gas responsible for the lines in the galactic disc. Fig. 6 is the *l–v* diagram of the H 272α lines observed in this survey in the range $l = 0°$ to 50°. This can be compared with *l–v* diagram for the 21 cm HI emission in the galactic plane (*e.g.* Lockman 1976). The HI emission occupies a much larger velocity range in such a diagram. It is therefore clear that the gas responsible for the low-frequency recombination line is not distributed like neutral hydrogen. This rules out the possibility that the line emitting regions are partially-ionized neutral-hydrogen clouds. This could be because ionization in the cold HI clouds is not adequate to produce detectable recombination lines at this frequency. Further, the width of these lines, which is in the range of 20–50 km s^{-1}, indicates that these lines do not arise from a distributed component of the interstellar medium.
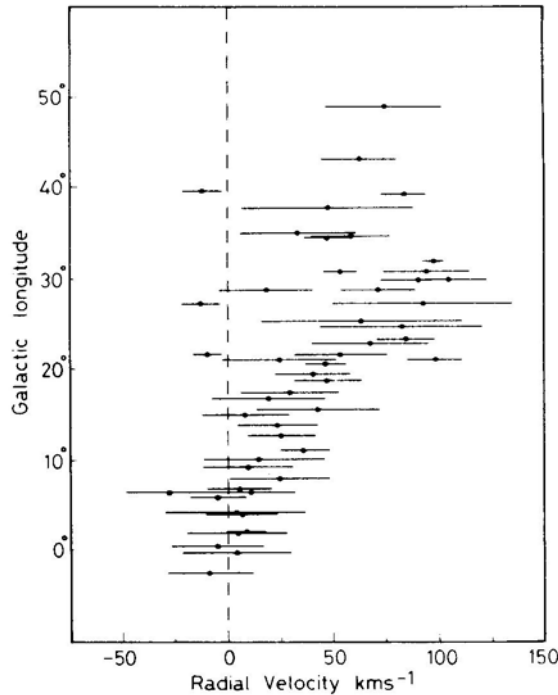
Figure 6. Longitude-velocity diagram of the observed H 272α lines. The extent of the horizontal lines indicates the observed half-power width and the dot indicates the centroid of the line.

On the other hand the l–v diagram in Fig. 6 is similar to those of HII regions seen in the H 110α survey (see Wilson 1980), the ionized galactic ridge seen in the H 166α survey (Lockman 1980), and molecular clouds seen in the CO surveys (Burton & Gordon 1978). The distributions of both HII regions and molecular clouds in the galactic disc show a peak between 4 kpc and 8 kpc from the galactic centre (Wilson 1980; Sanders 1983). While most of the recombination lines observed here do not arise in the HII regions seen in the H 110α survey, for reasons discussed earlier, the l–v diagram in Fig. 6 indicates that the lower-density gas responsible for these lines is distributed in a manner similar to HII regions and molecular clouds in the inner part of the Galaxy. As the H 272α recombination line is detected in every direction observed for $l < 40°$ representative quantities of low-density ionized gas must be present in every direction in this range.

6.2 *Carbon Lines*

Recombination lines of carbon are not as widespread as those of hydrogen. They have been detected at other frequencies in only 15 to 20 sources . To date these lines have been identified as coming from three types of regions. These are, the partially-ionized medium adjacent to HII regions (see Pankonin 1980), dark clouds surrounding early B-type stars (see Brown 1980) and possibly diffuse neutral hydrogen clouds (Konovalenko & Sodin 1981; Anantharamaiah, Erickson & Radhakrishnan 1985). The

Table 4. Observed parameters of carbon lines.

Source	T_L/T_C $\times 10^3$	Half-power width km s^{-1}	V_{LSR} km s^{-1}	Peak line temperature T_L (K)
G 359.9 − 0.0	0.71(06)	24(2.5)	0.0(1.0)	1.7(3)
G 0.7 − 0.0	0.58(09)	20(4)	3.5(2)	0.64(14)
G 4.4 + 0.1	0.70(13)	26(7)	8.5(3)	0.49(12)
G 7.0 − 0.3	1.0(2)	14(4)	5.5(2)	0.73(16)
G 14.0 − 0.1	1.1(1)	29(4)	27.5(2)	0.74(14)
G 17.6 − 0.3	0.32(08)	50(15)	20.5(6)	0.20(06)
G 19.6 + 0.0	0.67(14)	13(5)	49.5(2)	0.37(09)
G 23.4 − 0.2	0.93(13)	30(6)	85.5(2)	0.70(14)
G 24.8 + 0.1	0.73(09)	34(5)	45.5(2)	0.48(09)
G 34.7 − 0.6	0.69(13)	20(5)	17.5(2)	0.7(2)
G 37.8 − 0.2	1.2(2)	26(5)	53.5(2)	0.57(12)
G 206.8 − 16.4*	1.0(2)	26(7)	− 37.4(3)	0.12(03)

* Observation affected by interference.

carbon lines therefore arise in predominantly neutral and cool regions in contrast to hydrogen lines, most of which come from the hot fully-ionized HII regions.

In the present survey, C 272α line has been tentatively identified in 12 cases. The observed parameters are separately given in Table 4. For many of the sources, this is the first detection of a carbon line. The observed width of the lines (15–30 km s^{-1}) are much larger than those at higher frequencies (see for example Dupree 1974; Parrish & Pankonin 1975). If the large line widths are due to pressure broadening then electron densities of 50–100 cm^{-3} are implied for the regions. These in turn imply hydrogen densities of 2–3 $\times$ 10^5 cm^{-3}, if the cloud has normal interstellar abundance and all the carbon atoms are ionized. We note here that Silverglate & Terzian (1978) also report widths in excess of 25 km s^{-1} for carbon lines at 1400 MHz.

7. Summary

A survey of the H 272α recombination line has been made towards 53 directions in the galactic plane, consisting of 34 HII regions, 12 SNRs and 6 regions where the continuum is a minimum. Observed spectra and line parameters of the hydrogen lines detected towards 47 directions, and possible carbon lines towards 12 of these directions, are presented.

The H 272α line is seen in every direction observed with galactic longitude less than 40°. The line intensities are typically 0.1 per cent of the total continuum and there is no marked difference between directions of HII regions, SNRs and blank regions. Typical widths of the lines are 20–50 km s^{-1} but the lines are much wider in the longitude range 20° to 30°

The observed line temperatures show a good correlation with the total continuum temperature which is dominated by the nonthermal radiation at this frequency, indicating that the line intensities are enhanced by stimulated emission.

It is argued that these lines are unlikely to arise from typical HII regions (densities

> 100 cm^{-3}) which are prominent in many radio continuum surveys, due to the effects of pressure broadening, optical depth and beam dilution. These lines can arise only from much-lower-density gas. Judging from the velocity differences between H 110α lines, observed by Downes *et al.* (1980), and the present H 272α lines detected towards the same directions, there seems to be a physical association between the higher-density H II regions seen in H 110α and the lower-density gas responsible for the H 272α lines. The *l–v* diagram for these lines show that the distribution of this low-density gas is similar to that of H II regions and molecular clouds in the inner galactic disc, and is unlike that of neutral hydrogen which occupies a much larger velocity range. The widths of the lines indicate that the gas responsible for them is not a distributed component of the interstellar medium.

The observed widths of the carbon lines at 325 MHz are much larger than those at higher frequencies indicating that pressure broadening may have become important.

A more detailed and quantitative interpretation of the data presented in this paper will appear in the following paper (Anantharamaiah 1985).

Acknowledgements

References

Altenhoff, W. J., Downes, D., Pauls, T., Schraml, J. 1978, *Astr. Astrophys. Suppl.,* **35**, 23.
Anantharamaiah, K. R. 1985, *J. Astrophys. Astr.,* **6**, 203.
Anantharamaiah, K. R., Erickson, W. C, Radhakrishnan, V. 1985, *Nature,* **315**, 647.
Batty, M. J. 1976, *Aust. J. Phys.,* **29**, 419.
Bignell, R. C. 1973, *Astrophys. J.,* **186**, 889.
Brocklehurst, M., Leeman, S. 1971, *Astrophys. Lett.,* **9**, 35.
Brocklehurst, M, Seaton, M. J. 1972, *Mon. Not. R. astr. Soc.,* **157**, 179.
Brown, R. L. 1980, in *Radio Recombination Lines,* Ed. P. A. Shaver, D. Reidel, Dordrecht, p. 127.
Brown, R. L., Lockman, F. J., Knapp, G. R. 1978, *A. Rev. Astr. Astrophys.,* **16**, 445.
Burton, W. B., Gordon, M. A. 1978, *Astr. Astrophys.,* **63**, 7.
Cesarsky, D. A., Cesarsky, C. J. 1973, *Astrophys. J.,* **183**, L143.
Downes, D., Wilson, T. L. 1974, *Astr. Astrophys.,* **34**, 133.
Downes, D., Wilson, T. L, Bieging, J., Wink, J. 1980, *Astr. Astrophys. Suppl. Ser.,* **40**, 379.
Dulk, G. A., Slee, O. B. 1975, *Astrophys. J.,* **199**, 61.
Dupree, A. K. 1974, *Astrophys. J.,* **187**, 25.
Gordon, M. A., Cato, T. 1972, *Astrophys. J.,* **176**, 587.
Gordon, K. J., Gordon, C. P., Lockman, F. J. 1974, *Astrophys. J.,* **192**, 337.
Gordon, M. A., Gottesman, S. T. 1971, *Astrophys. J.,* **168**, 361.
Gottesman, S. T., Gordon, M. A. 1970, *Astrophys. J.,* **162**, L93.

Griem, H. R. 1967, *Astrophys. J.,* **148**, 547.

Hart , L., Pedlar, A. 1976, *Mon. Not. R. astr. Soc.,* **176**, 547.

Jackson, P. D., Kerr, F. J. 1975, *Astrophys. J.*, **196**, 723.

Konovalenko, A. A., Sodin, L. G. 1981, *Nature,* **294**, 135.

Lockman, F. J. 1976, *Astrophys. J.,* **209**, 429.

Lockman, F. J. 1980, in *Radio Recombination Lines,* Ed. P. A. Shaver, D. Reidel, Dordrecht, p. 185.

Matthews, H. E., Pedlar, A., Davies, R. D. 1973, *Mon. Not. R. astr. Soc.,* **165**, 149.

Pankonin, V. 1975, *Astr. Astrophys.,* **38**, 445.

Pankonin, V. 1980 in *Radio Recombination Lines,* Ed. P. A. Shaver, D. Reidel, Dordrecht, p. 111.

Pankonin, V., Parrish, A., Terzian, Y. 1974, *Astr. Astrophys.,* **37**, 411.

Parrish, A., Conklin, E. K., Pankonin, V. 1977, *Astr. Astrophys.,* **58**, 319.

Parrish, A., Pankonin, V. 1975, *Astrophys. J.,* **198**, 349.

Pedlar, A., Davies, R. D. 1980, in *Radio Recombination Lines,* Ed. P. A. Shaver, D. Reidel, Dordrecht, p. 171.

Pedlar, A., Davies, R. D., Hart, L., Shaver, P. A. 1978, *Mon. Not. R. astr. Soc.,* **182**, 473.

Reifenstein, E. C, Wilson, T. L., Burke, B. F., Mezger, P. G., Altenhoff, W. J. 1970, *Astr. Astrophys.,* **4**, 357.

Rieu, N.-Q. 1969, *Astr. Astrophys.,* **1**, 128.

Sarma , N. V. G., Joshi, M. R, Bagri, D. S., Ananthakrishnan, S. 1975, *J. IETE,* **21**, 110.

Shaver, P. A. 1975, *Pramana,* **5**, 1.

Shaver, P. A., Goss, W. M. 1970a, *Aust. J. Phys. Astrophys. SuppL.,* No. 14, 77.

Shaver, P. A., Goss, W. M. 1970b, *Aust. J. Phys. Astrophys. Suppl.,* No. 14, 133.

Silverglate, P. R., Terzian, Y. 1978, *Astrophys. J.,* **224**, 437.

Swarup , G., Sarma, N. V. G., Joshi, M. N., Kapahi, V. K., Bagri, D. S., Damle, S. H., Ananthakrishnan, S., Balasubramanian, V., Bhave, S. S., Sinha, R. P. 1971, *Nature,* **230**,185.

Terzian, Y., Pankonin, V. 1974, in *IAU Symp.* 60: *Galactic Radio Astronomy,* Ed. F. J. Kerr, & S. C. Simonson, p. 241.

Viner , M. R., Vallee, J. P., Hughes, V. A. 1979, *Astr. J.,* **84**, 1335.

Weinreb, S. 1962, *Technical Rep. No.* 412, Massachusetts Inst. Tech., Boston.

Wilson, T. L. 1980, in *Radio Recombination Lines,* Ed. P. A. Shaver, D. Reidel, Dordrecht, p. 205.